Pd Loaded TiO_2 Nanotubes for the Effective Catalytic Reduction of p*-Nitrophenol*

Vijila Kalarivalappil, C. M. Divya, W. Wunderlich, Suresh C. Pillai, Steven J. Hinder, Manoj Nageri, V. Kumar & Baiju K. Vijayan

Catalysis Letters

ISSN 1011-372X
Volume 146
Number 2

Catal Lett (2016) 146:474-482
DOI 10.1007/s10562-015-1663-8

Springer

Catal Lett (2016) 146:474–482
DOI 10.1007/s10562-015-1663-8

Pd Loaded TiO_2 Nanotubes for the Effective Catalytic Reduction of *p*-Nitrophenol

Vijila Kalarivalappil[1] · C. M. Divya[1] · W. Wunderlich[2] · Suresh C. Pillai[3,4] · Steven J. Hinder[5] · Manoj Nageri[1] · V. Kumar[1] · Baiju K. Vijayan[1]

Received: 14 August 2015 / Accepted: 17 November 2015 / Published online: 31 December 2015

Abstract Titania nanotubes decorated with Pd nanoparticles were synthesised by a hydrothermal method. The increased amounts of Pd concentration is found to facilitate the anatase to rutile crystalline phase transformation as well as in collapse of the morphology as revealed by X-ray diffraction, Raman spectroscopy, scanning and transmission electron microscopy. The presence of metallic as well as the oxidized form (PdO_2) of surface metal ions was characterized by using XPS. The catalytic activity of the Pd loaded titania nanotubes has been demonstrated by studying the reduction of *p*-nitrophenol to *p*-aminophenol. The 1.0 mol% Pd loaded titania nanotubes has been found to exhibit optimum catalytic activity (rate constant of 0.7072 min^{-1}) while those with higher amounts of Pd loading showed lower catalytic activity. It is observed that retention of tubular morphology and higher anatase content play significant roles in their catalytic activity.

Graphical Abstract

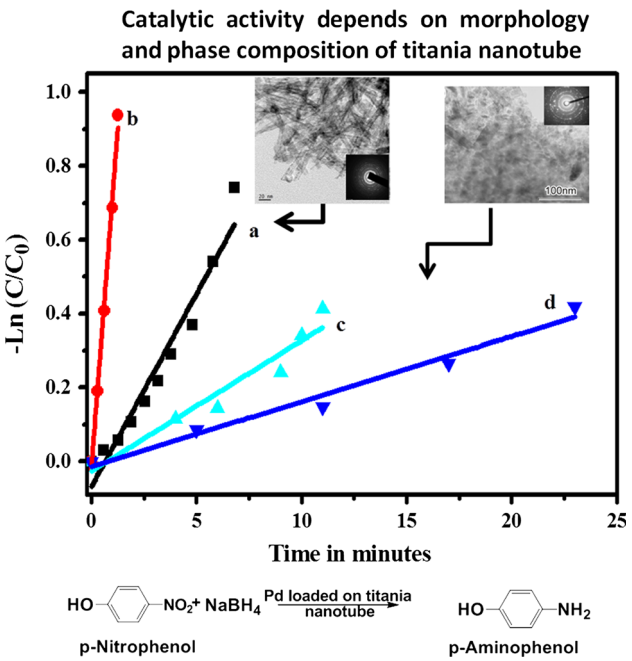

Key words Titania nanotubes · Anatase · Rutile · Morphology · Palladium · Catalysis and reduction

1 Introduction

Mesoporous titania finds applications in catalysis, photocatalysis, batteries, sensors and solar cells [1]. Strong oxidation and reduction power of photo generated reactive

Electronic supplementary material The online version of this article (doi:10.1007/s10562-015-1663-8) contains supplementary material, which is available to authorized users.

✉ Baiju K. Vijayan
baijuvijayan@gmail.com; baiju@cmet.gov.in

1 Department of Electronics and Information Technology, Centre for Materials for Electronics Technology (C-MET), Government of India, Shoranur Road, M. G. Kavu, Athani P.O., Thrissur, Kerala 680 581, India

2 Material Science Department, Faculty of Engineering, Tokai University, Kitakaname 4-1-1, Hiratsuka 259-1292, Japan

3 Nanotechnology Research Group, Department of Environmental Sciences, Institute of Technology Sligo, Sligo, Ireland

4 Centre for Precision Engineering, Materials and Manufacturing Research, Institute of Technology Sligo, Ash Lane, Sligo, Ireland

5 The Surface Analysis Laboratory, Department of Mechanical Engineering Sciences, University of Surrey, Guildford, Surrey GU2 7XH, UK

oxidation species (ROS) as a result of the photocatalytic reactions can effectively be used for decontamination and disinfection applications [2–8]. Titanium dioxide is identified as one of the most suitable candidates for catalytic reactions because of its chemical stability, nontoxicity and higher surface area [9]. Palladium (Pd) supported titania has been employed as catalysts for various reactions such as oxidative destruction of dichloromethane in presence of water vapour, methane combustion and ethanol oxidation in alkaline medium etc. [10–12]. A cost effective method for the synthesis of iron doped titania loaded with noble metals using industrial waste was reported by Mahmoud et al. [13]. Dichloromethane oxidation using titania doped with Pd and Ni was also reported [10]. Reduction of Pt(IV), Au(III) or Pd(II) doped titania under UV irradiation to metallic Pt, Au or Pd on the titania surface was reported [14]. Liquid phase selective hydrogenation of long chain alkadienes is also dependent on the catalytic activity of polymorphic phase of titania [15]. Palladium catalyst supported by anatase phase has shown higher selectivity compared with that of rutile phase supported materials [15]. The Pd and Pt doped titania have been effectively used for the inactivation of bacteria [16]. Pt and Pd deposited on titanate nanotubes have also been reported to be effectively used for hydrogen sensor applications. The sensor prepared with Pd and Pt/titanate nanotubes displayed improved response compared to the conventional Pd and Pt catalysts [17]. Pd deposited on titania nanofibers prepared by electrospinning technique have been reported to effectively catalyse the decomposition of NO and CO [18]. Pd deposited on grapheneoxide nanosheet shows greater catalytic properties for the reduction of *p*-nitrophenol than Au and Ag deposited [19]. Au, Pt and Pd supported on SBA-15 was used for catalytic reduction of *p*-nitrophenol. Among these Pd decorated material is more catalytically active than other metal nanoparticles [20]. However, a systematic study of Pd doping and its effect on the morphological stability and catalytic reduction of *p*-nitrophenol using Pd doped titania nanotubes has not yet been reported. In the current investigation Pd nanoparticles decorated titania nanotubes are prepared by hydrothermal technique. Various metal nanoparticles such as Ag, Au, Cu and Pd are used for the catalytic reduction of *p*-nitrophenol [21]. Pd is reported to be a better catalyst than the other similar metal [19, 20, 22]. Catalytic properties of palladium loaded titania nanotubes were systematically examined by studying the reduction of *p*-nitrophenol with sodium borohydride ($NaBH_4$) to *p*-aminophenol. The present work also aims at investigating the role of palladium nanoparticle loading on titania nanotubes on the catalytic reduction of *p*-nitophenol. The current investigation revealed that there is an optimum loading for metal nanoparticles to be more catalytically active.

2 Experimental

2.1 Chemicals Used

Chemicals and reagents such as anatase titania powder (assay 99 %, Merck), sodium hydroxide (assay 97 %, Merck), hydrochloric acid (assay 35 %, Merck), palladium (II) chloride (assay 99 %, Sigma Aldrich Chemicals), cetyltrimethyl ammonium bromide (assay 99 %, Sigma Aldrich Chemicals), hydrazine monohydrate (assay 98 %, Sigma Aldrich Chemicals, India), were used as such without any further purification.

2.2 Procedure

Titania nanotubes (TiNTs) were synthesized by using an improved hydrothermal method. In a typical reaction, 2 g of anatase titania powder were stirred with 50 ml of 10 M NaOH solution in a 125 ml Teflon cup (Paar Instrument Company, USA). This reaction system was retained in an oven for 48 h at 120 °C and the precipitate formed was washed with 1 M HCl. The reaction mixture was washed several times using deionized water to attain a pH between 6 and 7. The titania nanotubes thus synthesized were dried in a chamber oven at 110 °C for overnight. The Pd nanoparticles were prepared by chemical reduction method. In a typical experiment, 25 mM palladium (II) chloride was added drop-wise into a solution containing hyrazinemonohydrate (100 mM) and CTAB (0.5 M). After the addition of $PdCl_2$ the colour of the resultant solution changed to dark brown indicating the formation of Pd nanoparticles. This mixture was stirred for 10 min, it is further used for loading Pd nanoparticles in titania nanotubes matrix. Palladium concentrations of 0.1, 1, 5, 10 mol% loaded over hydrogen titanate nanotubes by adding drop-wise of Pd nanoparticles suspension into an aqueous suspension of hydrogen titanate nanotube under stirring. The resultant slurry dried and further calcined at 400 °C for 1 h. The samples were coded as 0.1Pd, 1Pd, 5Pd and 10Pd in following tests. The concentration of Pd in the respective samples also measured using SEM EDAX analysis. The phase identification were carried out using X-ray diffractometer (D5005, Bruker, Germany) using Cu Kα radiation of 0.15406 nm at the scanning rate 0.05°/s in the 2θ range from 5° to 80°. The amount of rutile in the sample was estimated by using the Spurr calculations (Eq. (1).

$$\% \text{ Rutile} = \frac{1}{1 + 0.8[I_A(101)/I_R(110)]} \quad (1)$$

where I_A (1 0 1) and I_R (1 1 0) are the integrated main peak intensities of anatase and rutile respectively. The Scherrer formula was used to estimate the average particle size of the Pd nanoparticle (Eq. 2).

$$D = \frac{K\lambda}{\beta \cos\theta} \quad (2)$$

where D is the average particle size (nm), K, the shape factor, λ the X-ray wavelength (1.5406 Å), β is the full width at half maximum (in radian) of (111) peak of metallic Pd and θ is the Bragg angle.

The morphology of the materials was monitored using field emission scanning electron microscope (Hitachi SU6600, USA) and high resolution transmission electron microscope (Hitachi HF 2200 TU (Japan). The catalytic performance of the titania nanotube loaded with palladium was quantitatively evaluated in the liquid-phase reduction of *p*-nitrophenol (4-NP) with sodium borohydride ($NaBH_4$). The reaction is known to be catalytically active in presence of metal nanoparticles at room temperature. In a typical experiment an aqueous solution of *p*-nitrophenol (0.01 M; 20 ml) and sodium borohydride (0.5 M; 20 ml) were prepared and from their mixture 0.12 ml is pipetted out to quartz cuvette and diluted with 3.8 ml water. 1 mg of each prepared sample of palladium loaded titania nanotubes (0.1 Pd, 1 Pd, 5 Pd and 10 Pd) is added into it and stirred. Then this mixture is transferred into a UV–Visible spectrometer (Perkin Elmer, Lambda 35, USA). *P*-nitrophenol exhibits an absorption peak at 317 nm. Addition of $NaBH_4$ deprotonates the OH group of *p*-nitrophenol, and subsequently the absorption peak shifts to 400 nm. When the catalytic reduction of *p*-nitrophenol is initiated the peak gradually reduces its intensity. In the meantime a small shoulder peak at 300 nm gradually rises, which is attributed to *p*-amino phenol [22]. The recyclability of the catalysts was also analyzed after the reaction. The time dependant absorption spectra of the *p*-nitrophenol reaction solution in presence of 1Pd catalyst in 2nd and 3rd cycle are provided in the supplementary Information Fig. 1. XPS analyses were performed on a ThermoFisher Scientific (East Grinstead, UK) Theta Probe spectrometer. XPS spectra were acquired using a monochromated Al Kα X-ray source (hυ = 1486.6 eV). An X-ray spot of 400 μm radius was employed. All spectra were charge referenced against the C1s peak at 285 eV to correct for charging effects during acquisition. Quantitative surface chemical analyses were calculated from the high resolution, core level spectra following the removal of a non-linear (Shirley) background. The manufacturers Advantage software was used which incorporates the appropriate sensitivity factors and corrects for the electron energy analyser transmission function.

3 Results and Discussion

The X-ray diffraction patterns of the samples (Fig. 1) calcined at 400 °C shows crystalline peaks corresponding to the anatase crystalline phase of titania. At higher loading

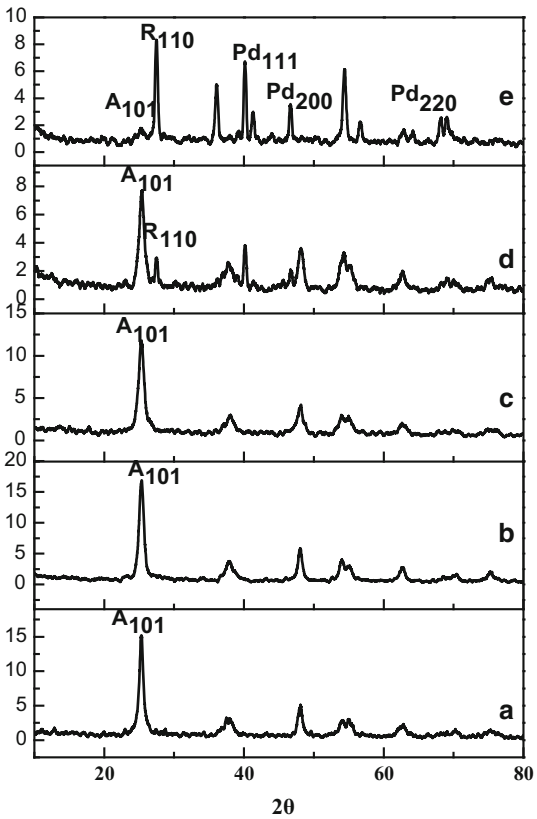

Fig. 1 XRD pattern of pure and Pd loaded titania nanotube calcined at 400 °C *a* NT, *b* 0.1 Pd, *c* 1 Pd, *d* 5 Pd and *e* 10 Pd

of Pd such as 5 and 10 mol%, crystallization of 32 and 85 % of rutile phases respectively, were observed. In 5Pd and 10 Pd samples the peaks at 2θ = 40, 46.4, 68.2 correspond to the (111), (200), (220) planes of fcc structured Pd particles [23]. It was reported that Pd in the titania matrix favours the anatase to rutile phase transformation [24]. The ionic radius of Pd is 137 pm, which is significantly larger than that of Ti^{4+} ion (68 pm). Therefore, it is difficult to replace titanium ion with Pd in the lattice of anatase structure. However, the increase in oxygen vacancy in the titania lattice was reported to enhances the anatase to rutile phase transformation. [24, 25] The average crystallite size of Pd is found to be 19.6, 20.3 nm for 5Pd and 10Pd samples. The concentration of Pd in the titania matrix as determined using EDAX measurement are found to be 1.56, 2.70, 3.22 and 6.07 wt% for 0.1Pd, 1Pd, 5Pd, 10Pd samples respectively.

Raman spectra of the Pd loaded and unloaded titania nanotubes are provided in Fig. 2. In pure, 0.1Pd and 1Pd samples, phonon modes corresponding to anatase type are present at 144, 197, 399, 513 and 639 cm^{-1}. [26, 27]. Phonon modes corresponding to the rutile phase of titania are observed for 5Pd and 10Pd samples at 608, 392 and 247 cm^{-1}. Results obtained from the Raman spectra (Fig. 2) are in conformity with those obtained from XRD.

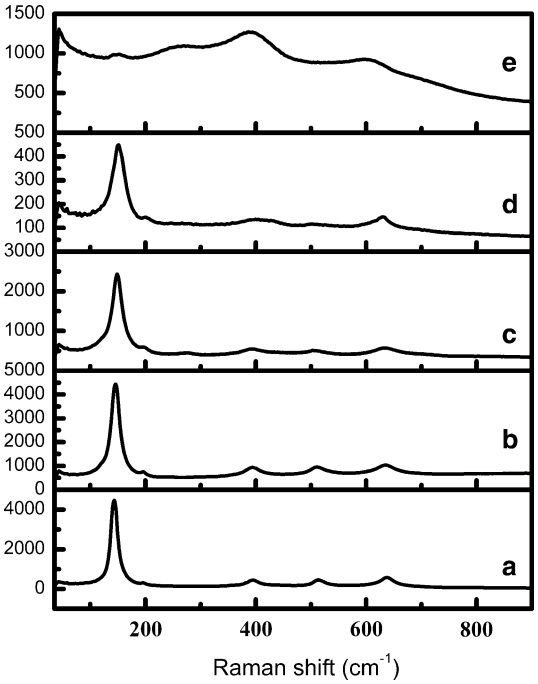

Fig. 2 Raman spectra of Pd loaded and unloaded titania nanotube *a* NT, *b* 0.1 Pd, *c* 1 Pd, *d* 5 Pd and *e* 10 Pd

The scanning electron microscope images of the samples indicate a tubular morphology of the titania nanotube samples up to a Pd concentration of 1.0 mol% (Fig. 3a–c). As the Pd concentration increases (Fig. 3d, e) collapse of the tubular structure in titania nanotubes is observed which is attributed to anatase to rutile phase transformation [28].

In titania nanotube with 0.1 and 1.0 mol% Pd, transmission electron microscope images (Fig. 4) reveal tubular morphology with an average diameter between 10 and 12 nm (Figs. 4a, b). HRTEM reveals multi wall tube structure that shows signs of scrolling during formation of titania nanotubes synthesised through hydrothermal method (Fig. 4c) [29]. Pd particles can be distinguished from the dominant anatase phase because of their dark contrast. The particle size of the Pd particle is measured through TEM analysis indicates that 0.1Pd and 1 Pd sample have an average particle size of 11 and 13 nm respectively. At higher loading such as 5 mol% of Pd, the tubular morphology crumbled to nanopowder (Figs. 4d). The selected area electron diffraction pattern of the samples (insets of Figs. 4a, b, d) clearly indicate that the 0.1 and 1Pd samples are less crystalline in nature than the 5 Pd sample, mainly caused by the nanotubes with high aspect ratio. The BET surface area obtained are 240, 261, 228, 167 and 159 m^2g^{-1} for pure and Pd loaded titania nanotube samples such as 0.1 Pd, 1 Pd, 5 Pd 10 Pd respectively. The drastic reduction in the surface area of the 5 and 10 Pd samples indicate the collapse of tubular structure of highly Pd loaded samples.

The XPS spectra of the Ti 2*p* peak are provided in the Fig. 5a. The Ti 2*p* 3/2 peak in TiO_2 reported to be observed at 458.8 eV [30]. The binding energy of 2*p* peak of titania is increased from 458.68 to 459.23 when the concentration of Pd increases in the titania matrix. Peak shift is detected which indicates decrease of the coordination number of Ti and the shortening of the Ti–O bond [31]. Lower binding energies of Ti 2*p* 3/2 is a good indication of the lowering of valence state level of Ti $^{4+}$ to Ti $^{3+}$ [31] and the formation of oxygen vacancy in the system [32]. This enhances the anatase to rutile phase transformation in Pd loaded titania nanotube. The O1*s* binding energy of TiO_2 has been reported to be observed at 529.9 eV (Fig. 5b) [33]. Moreover, the asymmetry in the oxygen peak indicates different chemical states of oxygen. The binding energy of oxygen in PdO is reported between 529.8–530.1 eV [34].

The XPS spectra of Pd 3d peak are presented in Fig. 5c, in which the palladium exists in metallic as well as PdO_2 state. The presence of metallic as well as oxidized form (PdO_2) are characterized by the binding energies at 340.7 eV ($3d_{3/2}$), 335.5 eV ($3d_{5/2}$) for Pd [30] where as for PdO_2, they are at 342.8 eV ($3d_{3/2}$) and 337.7 eV ($3d_{5/2}$) [35]. The XPS spectra of the Pd 3d peak for all of the Pd loaded samples are provided in the supplementary Fig. 2. According to the XRD data, the Pd exists in metallic state even though the XPS data show peaks corresponding to oxidized palladium species PdO_2. This discrepancy can be explained by the low stability of the reduced palladium states. It is reported that PdO_2 particles have been shown to be stabilized by the matrix of other oxides, such as Al_2O_3 and SnO_2 [36, 37]. However the X-ray diffraction indicates only the presence of metallic palladium. This discrepancy is likely to arise from the very different depths of analysis between the two techniques. In X-ray diffraction analysis penetration/analysis depth is reported to be of few microns [38] whilst XPS has an analysis depth below 10 nm [39]. Thus a thin layer of Pd oxide on the surface of Pd will show as a major contribution to the XPS Pd peak and remain undetected, via X-ray diffraction analysis.

The catalytic action of Pd loaded titania nanotube were studied using liquid phase reduction of *p*-nitrophenol by sodium borohydride. The reduction of *p*-nitrophenol to *p*-aminophenol using sodium borohydride is usually accelerated in the presence of a metal catalyst [40, 41]. The reduction pathway is depicted in Eq. 3. The catalytic reduction in presence of excess sodium borohydride has been reported to follow first order kinetics. Figure 6a represents a typical plot of the time dependent absorption spectra of *p*-nitrophenol in presence of Pd loaded titania nanotube. The reduction was monitored from the decrease in the absorption maximum of *p*-nitrophenol at 400 nm [42, 43] and the increase in intensity of the peak at 300 nm corresponding to the formation of *p*-aminophenol. A small

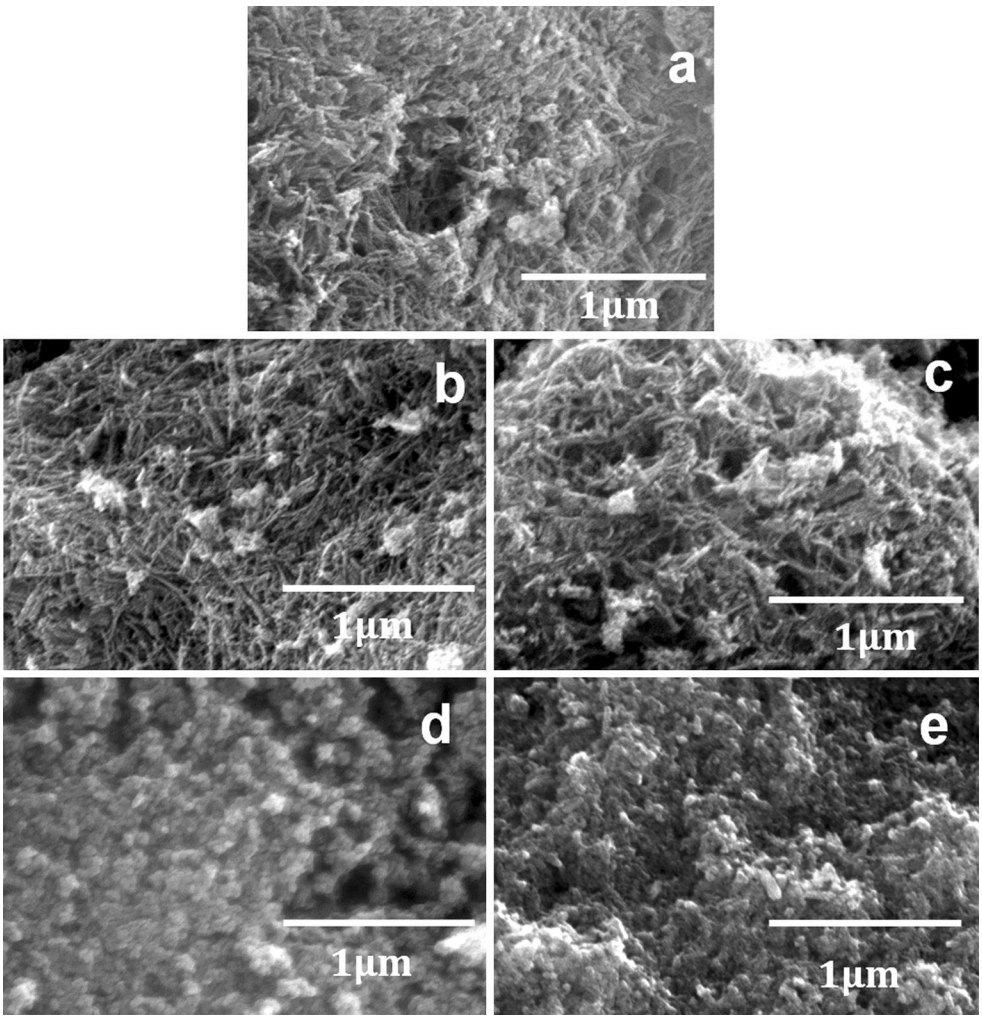

Fig. 3 SEM images of pure and Pd loaded titania nanotubes calcined at 400 °C **a** NT, **b** 0.1 Pd, **c** 1 Pd, **d** 5 Pd and **e** 10 Pd

reduction in concentration of *p*-nitrophenol with pure titania nanotube powder was also observed (supplementary information Figure S3). Which may be due to the adsorption of reactant on titania nanotube surface or the slow reduction of *p*-nitrophenol by sodium borohydride in the absence of metal catalyst [44]. This shows that pure titania cannot alone accelerate the catalysis reaction. In order to quantify the catalytic action of different samples, reaction kinetics for the reduction of *p*-nitrophenol in presence of Pd loaded titania nanotube catalyst are studied. Figure 6b shows the typical plot of $-\ln(c_{(t)}/c_{(0)})$ against time, where $c_{(t)}$ and $c_{(0)}$ are the concentrations of *p*-nitrophenol at time t and 0, respectively. From the slope of the linear fit the rate constant of the reaction was calculated. The rate constants of the 0.1 Pd, 1 Pd, 5 Pd and 10 Pd samples are 0.0894, 0.7072, 0.0324, 0.0168 min^{-1} respectively. The rate constant of the reaction follows the following order: 1Pd > 0.1Pd > 5Pd > 10Pd. The presence of Pd particles on titania matrix catalyse the reduction reactions. Even though 5 Pd and 10 Pd contain higher amounts of palladium, they show lower catalytic reaction. There are two possible mechanisms for the reduction of *p*-nitrophenol (1) surface mediated electron transfer and (2) surface mediated hydrogen transfer. In both these mechanisms the reactants are adsorbed on the surface of the metal nanoparticle before the reduction reaction. Hence the surface area of the metal plays a major role in the reduction reaction. The reduction of *p*-nitrophenol has been reported to be kinetic and diffusion controlled. In diffusion controlled reactions, since the reactions on the surface of metal particles are significantly faster than diffusion of the reactants, apparent rate constant is determined by the diffusion of the reactants through the solution. The molecular size of the 4-NP calculated using molecular modeling is reported to be 6.6 Å by 4.3 Å in the plane of the benzene ring [45]. This indicates that the tubular structure and surface area have very important role in the catalytic reaction. The titania nanotubes synthesized in the present method have inner

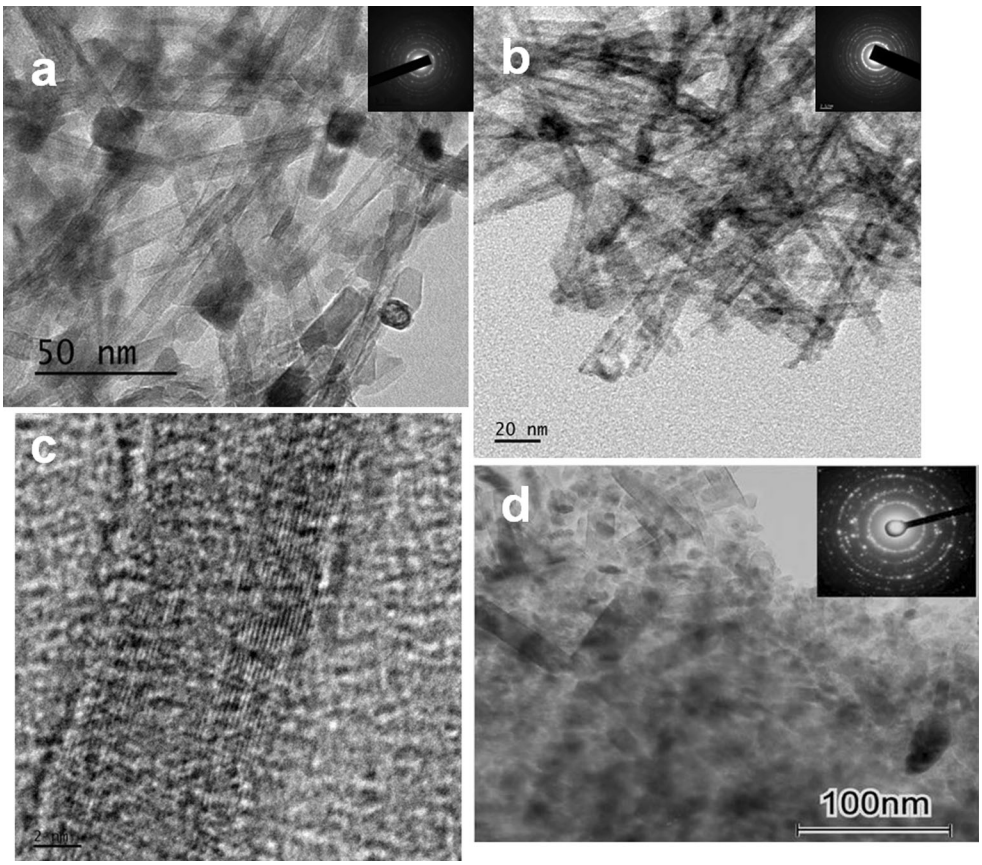

Fig. 4 TEM images of Pd loaded titania nanotubes calcined at 400 °C **a** 0.1 Pd, **b**, **c** 1 Pd, **d** 5 Pd

diameters of 6.0–7.0 nm (Fig. 4c), which allow the easy diffusion of reactants through the heterogeneous catalysis system. This facilitates the higher rate constant for the system with stable tubular structure containing lower concentration of palladium nanoparticles. The XPS result indicates the formation of Pd and PdO_2 in the samples. Earlier work indicated that both the metallic as well as the oxide form of palladium contribute to the reduction reaction of 4-NP [46]. Moreover, the reaction rates of different prepared samples reveal that, for a higher catalytic action there is an optimum Pd loading level. In the case of higher loading of Pd in the titania matrix for 5 and 10 Pd samples, even though the variation of particle size is very less, the 5 Pd exhibits a two times higher rate constant than 10 Pd sample. This clearly indicate that not only morphology but phase composition of titania matrix also has a significant effect on the reduction of *p*-nitrophenol. The 10 Pd sample contains 85 % of rutile whereas 5 Pd has 32 % rutile phase. In the present case we could see that the optimum level concentration is 1 mol% Pd loading (1Pd). Above and below this concentration the rate of reaction decreases in Pd loaded titania nanotubes. The smaller particles contain more exposed surface atom due to high surface to volume ratio and which will exhibit more catalytic active sites. However, it is reported that intermediate size is more catalytic active for the para nitro phenol reduction reaction [47]. Therefore, morphology and the nature of the substrate as well as particle size of Pd have played a major role in the reduction reaction as reported earlier [22].

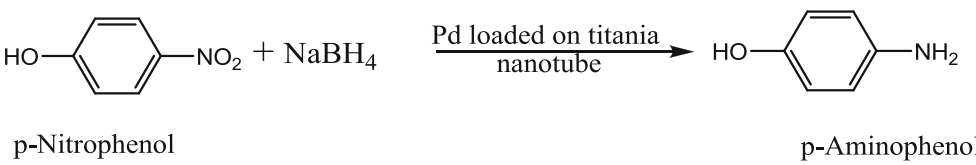

p-Nitrophenol p-Aminophenol (3)

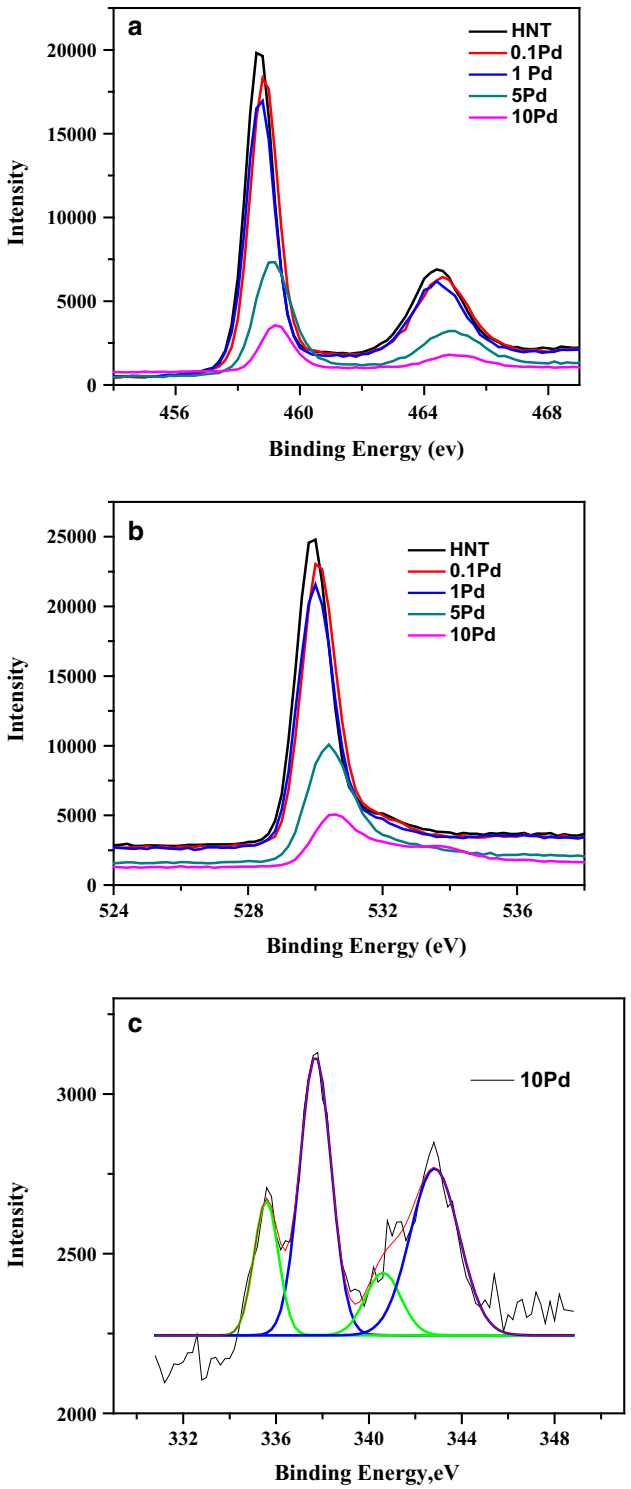

Fig. 5 XPS spectra of Pd doped titania nanotube samples **a** Ti 2p, **b** O1s, **c** Pd 3d of 10 Pd sample

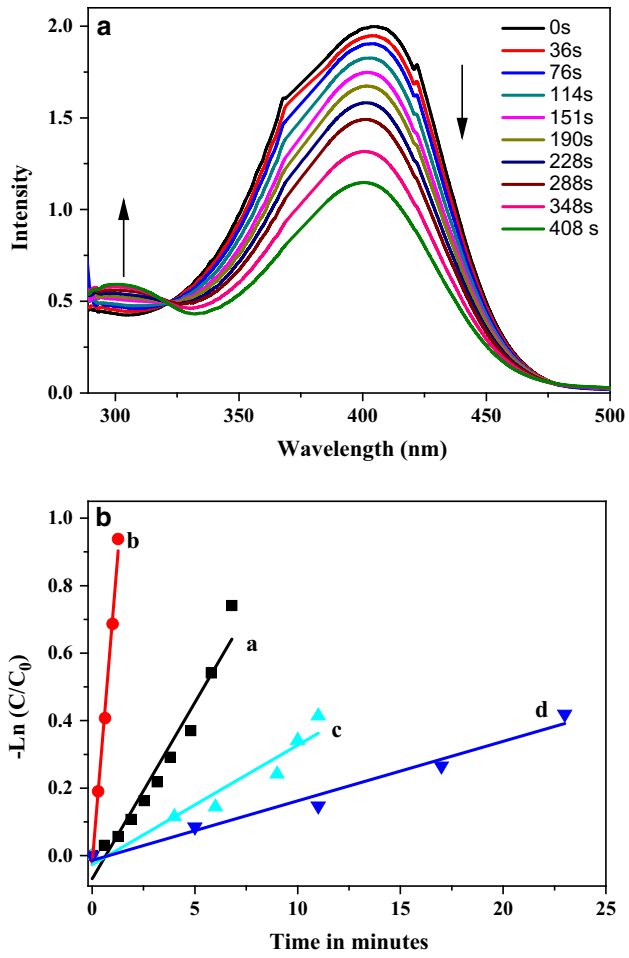

Fig. 6 **a** Time dependent absorption spectra of the reaction solution in the presence of the Pd loaded titania nanotube (0.1 Pd), **b** a typical plot of $-\ln (C/C_0)$ against time for the determination of rate constant for reduction of *p*-nitrophenol by $NaBH_4$ in presence of Pd loaded titania nanotube catalyst (*a*) 0.1 Pd (*b*) 1 Pd (*c*) 5 Pd and (*d*) 10 Pd

Though size of the metal nanoparticles are known to significantly influence the catalytic activity [48, 49] in the present case, the morphology as well as the crystalline phase of the host titania nanotube are found to play important roles in their catalytic activity. The comparison of the result with the published literature on catalytic reduction of *p*-nitrophenol using Pd nanoparticle supported on different substrates is provided in Table 1. It is clearly seen that the present method provides an easy and scalable method for the synthesis of Pd supported titania nanotube catalyst for the reduction of *p*-nitrophenol to *p*-aminophenol. The product has applications in production of analgesic, antipyretic drugs, photographic developers, corrosion inhibitors and anticorrosion lubricants. The rate of the reaction is comparable with the rate constant reported by other groups using Pd catalyst (Table 1). A rate constant of 0.7072 min^{-1} was obtained at a concentration 0.01 M of 4-NP using 1 mg of catalyst containing 1 mol% Pd nanoparticle, which is higher than many of the reported values presented in the Table 1. Therefore the current method holds promise for the industrial production of efficient catalyst for the reduction of *p*-nitrophenol in bulk quantities.

Table 1 Catalytic activity comaprison of Pd nanoparticle supported on different material for the reduction of 4-nitro phenol (4-NP)

Nature of the catalyst	Rate constant	Amount of catalyst	Concentration of 4-nitrophenol (4-NP)	References
Pd supported on titania microspheres	0.19 min^{-1}	1 mol% Pd on titania microsphere of wt% 0.02–0.7 mg	10×10^{-3} M	Zhao Jin et al. [22].
Pd on partially reduced graphene oxide	2.40×10^{-1} s^{-1} (14.4 min^{-1})	3 mg of reduced grapheme oxide contain a 10 mM concentration of Pd	10×10^{-3} M	Min-Quan Yang et al. [19].
Pd immobilized on Multiwalled carbon nanotube bonded with amphilic dendrimer	0.0141 min^{-1}	2.5 mg of functionalized multiwalled carbon nanotube containing 17.7 wt% Pd nanoparticle of size 3.8 nm	6×10^{-5} M	E. Murugan et al. [53].
Palladium nanoparticles stabilized by glycodendrimers in water	4×10^{-3} S^{-1} (0.24 min^{-1})	0.2 mol% gycodendrimer–Pd contains 1.4×10^{-4} M Pd	2.5×10^{-4} M	Sylvain Gatard et al. [54]
PPI dendrimer-palladium nanocomposites	4074×10^{-4} S^{-1} (24.444 min^{-1})	2 mmol of PPI dendrimer containing pd nanoparticle of size 2 nm	2×10^{-3} M	Kunio Esumi et al. [55]
Current study	0.7072 min^{-1}	1 mg of 1 mol% of Pd in titania nanotube matrix	10×10^{-3} M	

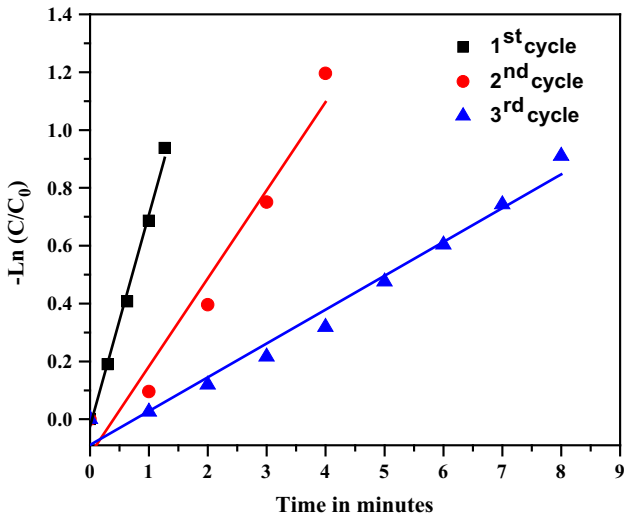

Fig. 7 A typical plot of $-\ln (C/C_0)$ against time for the determination of rate constant for reduction of *p*-nitrophenol by $NaBH_4$ in presence of 1 Pd (recyclability) (*square*) 1st cycle (*circle*) 2nd cycle and (*triangle*) 3rd cycle

The recyclability of the catalyst were monitored by repeating the *p*-nitrophenol reduction reaction for 2nd and 3rd cycle with 1 Pd sample, which have a rate constant of 0.7072 min^{-1} for *p*-nitrophenol reduction in 1st cycle (Fig. 7). After consecutive cycles catalytic activity of *p*-nitrophenol reduction reaction with 1 Pd sample the decreased drastically. It was previously noted that the catalytic activity could significantly be reduced in noble metals due to aggregation and leaching of the noble metal in the reaction mixture [50]. To improve the recyclability a core shell approach has previously been successfully tried with ceria and carbon [51, 52]. Zhang et al. reported a high catalytic deactivation for reduced grapheme oxide @ Pd catalyst after 10 cycles. They observed that the time required for 100 % conversion of *p*-nitrophenol increases from 25 s in 1st cycle to 420 s after 10th cycle [52]. In the current investigation a decrease in the rate constant to 0.2641 and 0.1013 min^{-1} in 2nd and 3rd cycle has been observed. Further investigation is required to improve the recyclability of the catalyst.

4 Conclusions

The catalytic performance of palladium loaded titania was quantitatively evaluated in the liquid-phase reduction of *p*-nitrophenol by sodium borohydride. The 1 mol% Pd loaded titania nanotubes exhibit maximum catalytic efficiency for the catalytic reduction of *p*-nitro phenol to *p*-amino phenol. An apparent rate constant of 0.7072 min^{-1} was observed in the 1Pd sample for the catalytic reduction. The morphology as well as the crystalline phase of the titania nanotube are found to play important roles in their catalytic activity The Pd loaded titania nanotubes will be useful for highly efficient catalysts for industrially important chemical reactions. The recyclability of the catalyst were also monitored and found that the rate constant reduces to 0.2641 and 0.1013 min^{-1} in 2nd and 3rd cycles respectively.

Acknowledgments The authors acknowledge financial support from DST-SERB fast track (SR/FT/CS-122/2011). VK and MN acknowledge UGC for research fellowship. SP wishes to acknowledge financial support from the U.S. Ireland R&D Partnership Initiative, Science Foundation Ireland (SFI-Grant Number 10/US/I1822 (T)).

References

1. Zhang R, Elzatahry AA, Al-Deyab SS, Zhao D (2012) Nano Today 7:344
2. Hamilton JWJ, Byrne JA, Dunlop PSM, Dionysiou DD, Pelaez M, O'Shea K, Synnott D, Pillai SC (2014) J Phys Chem C 118:12206
3. Keane DA, McGuigan KG, Ibanez PF, Polo-Lopez MI, Byrne JA, Dunlop PSM, O'Shea K, Dionysiou DD, Pillai SC (2014) Catal Sci Technol 4:1211
4. Vijayan BK, Dimitrijevic NM, Wu J, Gray KA (2010) J Phys Chem C 114:21262
5. Vijayan BK, Dimitrijevic NM, Rajh TK, Gray K (2010) J Phys Chem C 114:12994
6. Baiju KV, Shajesh P, Wunderlich W, Mukundan P, Kumar SR, Warrier KGK (2007) J Mol Catal A: Chem 276:41
7. Baiju KV, Periyat P, Pillai PK, Mukundan P, Warrier KGK, Wunderlich W (2007) Mater Lett 61:1751
8. Banerjee S, Dionysiou DD, Pillai SC (2015) Appl Catal B 176–177:396
9. Banerjee S, Pillai SC, Falaras P, O'Shea KE, Byrne JA, Dionysiou DD (2014) J Phys Chem Lett 5:2543
10. Martínez LM, de Correa MTC, Odriozola JA, Centeno MA (2006) J Mol Catal A: Chem 253:252
11. Kang TG, Kim JH, Kang SG, Seo G (2000) Catal Today 59:87
12. Hu F, Ding F, Song S, Shen PK (2006) J Power Sour 163:415
13. Mahmoud MHH, Ismail AA, Sanad MMS (2012) Chem Eng J 187:96
14. Zheng S, Gao L (2003) Mater Chem Phys 78:512
15. Li Y, Xu B, Fan Y, Feng N, Qiu A, He JMJ, Yang H, Chen Y (2004) J Mol Catal A: Chem 216:107
16. Quisenberry LR, Loetscher LH, Boyd JE (2009) Catal Commun 10:1417
17. Han CH, Hong DW, Kim IJ, Gwak J, Han SD, Singh KC (2007) Sens Actuators B 128:320
18. Shahreen L, Chase GG, Turinske AJ, Nelson SA, Stojilovic N (2013) Chem Eng J 225:340
19. Yang MQ, Pan X, Zhang N, Xu YJ (2013) Cryst Eng Commun 15:6819
20. El-Sheikh SM, Ismail AA, Al-Sharab JF (2013) New J Chem 37:2399
21. Pradhan N, Pal A, Pal T (2001) Langmuir 17:1800
22. Jin Z, Xiao M, Bao Z, Wang P, Wang J (2012) Angew Chem Int Ed 51:6406
23. Teranishi T, Miyake M (1998) Chem Mater 10:594
24. Hanaor DH, Sorrell C (2011) J Mater Sci 46:855
25. Hishita S, Mutoh I, Koumoto K, Yanagida H (1983) Ceram Int 9:61
26. Ohsaka T, Izumi F, Fujiki Y (1978) J Raman Spectrosc 7:321
27. Berger H, Tang H, Lévy F (1993) J Cryst Growth 130:108
28. Asthana A, Shokuhfar T, Gao Q, Heiden PA, Friedrich C, Yassar RS (2010) Adv Sci Lett 3:557
29. Wang YQ, Hu GQ, Duan XF, Sun HL, Xue QK (2002) Chem Phys Lett 365:427
30. Moulder JF, Stickle WF, Sobol PE, Bomben KD (1992) Hand book of X-ray electron spectroscopy, Perkin-Elmer Corporation, Physical Electronics Division, Eden Prairie, United Stales of America 72–73
31. Etacheri V, Seery MK, Hinder SJ, Pillai SC (2011) Adv Funct Mater 21:3744
32. Xiao P, Fang H, Cao G, Zhang Y, Zhang X (2010) Thin Solid Films 518:7152
33. Carley AF, Roberts JC, Roberts MW (1990) Surf Sci 225:L39
34. Westerstrom R, Messing ME, Blomberg S, Hellman A, Gronbeck H, Gustafson J (2011) Phys Rev B 83:115440
35. Kim KS, Gossmann AF, Winograd N (1974) Anal Chem 46:197
36. Otto K, Haack LP, deVries JE (1992) Appl Catal B 1:1
37. Domashevskaya EP, Ryabtsev SV, Turishchev SY, Kashkarov VM, Yurakov YA, Chuvenkova OA, Shchukarev AV (2008) J Struct Chem 49:80
38. Guinebretiene R (2006) X-ray diffraction by polycrystalline materials. Cachan, Lavoisier
39. Gilbert JB, Rubner MF, Cohen RE (2013) Proc Natl Acad Sci USA 110:6651
40. Zeng J, Zhang Q, Chen J, Xia Y (2009) Nano Lett 10:30
41. Ge J, Zhang Q, Zhang T, Yin Y (2008) Angew Chem Int Ed 47:8924
42. Wu SH, Tseng CT, Lin YS, Lin CH, Hung Y, Mou CY (2011) J Mater Chem 21:789
43. Endo T, Yoshimura T, Esumi K (2005) J Colloid Interface Sci 286:602
44. Singla ML, Negi A, Mahajan V, Singh KC, Jain DVS (2007) Appl Catal A 323:51
45. Huang J, Yan C, Huang K (2009) J Colloid Interface Sci 332:60
46. Javaid R, Kawasaki SI, Suzuki A, Suzuki TM (2013) Beilstein J Org Chem 9:1156
47. Fenger R, Fertitta E, Kirmse H, Thunemann AF, Rademann K (2012) Phys Chem Chem Phys 14:9343
48. Johnson JA, Makis JJ, Marvin KA, Rodenbusch SE, Stevenson KJ (2013) J Phys Chem C 117:22644
49. Panigrahi S, Basu S, Praharaj S, Pande S, Jana S, Pal A, Ghosh SK, Pal T (2007) J Phys Chem C 111:4596
50. Zhang N, Xu Y-J (2013) Chem Mater 25:1979
51. Yu T, Zeng J, Lim B, Xia Y (2010) Adv Mater 22:5188
52. Zhang Z, Xiao F, Xi J, Sun T, Xiao S, Wang H (2014) Sci Rep 4:4053
53. Murugan E, Vimala G (2013) J Colloid Interface Sci 396:101
54. Gatard S, Salmon L, Deraedt C, Ruiz J, Astruc D, Bouquillon S (2014) Eur J Inorg Chem 2014:4369
55. Esumi K, Isono R, Yoshimura T (2004) Langmuir 20:237